High-Resolution Surface Plasmon Imaging of Gold Nanoparticles by Energy Filtered Transmission Electron Microscopy

Bernhard Schaffer,[1,2,3] Ulrich Hohenester,[4] Andreas Trügler,[4] and Ferdinand Hofer[1]

[1]*Institute for Electron Microscopy and Fine Structure Research, Graz University of Technology, 8010 Graz, Austria*

[2]*SuperSTEM Laboratory, STFC Daresbury, Keckwick Lane, WA4 4AD, Warrington, United Kingdom*

[3]*Department of Physics and Astronomy, University of Glasgow, G12 8QQ, Glasgow, United Kingdom*

[4]*Institut für Physik, Karl–Franzens–Universität Graz, Universitätsplatz 5, 8010 Graz, Austria*

(Dated: December 2, 2008)

Abstract

We demonstrate the imaging capabilities of energy-filtered transmission electron microscopy at high energy resolution in the low energy-loss region, reporting the first direct image of a surface plasmon of an elongated gold nanoparticle at energies around 1 eV. Using complimentary model calculations performed within the boundary element method approach we can assign the observed results to the plasmon eigenmodes of the metallic nanoparticle.

PACS numbers: 73.20.Mf, 79.20.Uv, 68.37.Og, 78.20.Bh

Plasmonics is an emerging field with numerous applications [1, 2], ranging from optical data processing [3, 4] over negative-refraction materials [5, 6] to bio-sensors [7, 8]. Surface plasmons, the workhorse of plasmonics, allow to bridge between the micro- and nanometer length scales of conventional optics and nano-devices. This is achieved by binding or converting light to coherent electron charge oscillations, confined to the surface of metallic nanostructures. When optical emitters, such as molecules or quantum dots, are placed in the vicinity of metallic nanoparticles, they couple strongly to the evanescent fields of the surface plasmons, and the light-matter coupling becomes significantly enhanced. This is exploited in surface enhanced Raman scattering [9] or surface enhanced fluorescence [10], as well as in single-plasmon generation [11].

The electromagnetic enhancement is particularly strong at the so-called "hot spots", with typical sizes of a few nanometers, which are usually located in the gaps between two nanoparticles or at the sharp edges of single particles. While enhancement factors of several orders of magnitude are predicted [12], the analysis of the experimental data is often cumbersome and controversial due to the limited spatial resolution provided by optical far- and nearfield techniques, as well as due to the uncertainties regarding the precise location of the optical emitters. An alternative experimental technique, which allows to bypass these difficulties, is electron energy-loss spectroscopy (EELS) in combination with scanning transmission electron microscopy (STEM) [13]. Here, a high-energy electron beam, with a transversal extension on the sub-nanometer scale, passes in the vicinity or through the nanoparticle, and some electrons lose energy through plasmon excitations, which are subsequently monitored. By raster scanning the beam over the metallic nanoparticle, one obtains information about the photonic local density of states of the metallic nanoparticles [13–17]. The spatial resolution of the maps is limited to the nanometer range by delocalization of the inelastic scattering [18, 19].

The drawbacks of the EELS technique have so far been the energy cutoff in the low-energy regime and the limited spatial resolution in large-area mappings. On the one hand, the so-called zero-loss peak (ZLP) of the electron beam usually masks the low-energy part of the spectrum. This hinders the direct observation of surface plasmons in the red and infrared regime, which is particularly appealing for (bio)sensors or applications at the telecom wavelengths. On the other hand, as STEM EELS data are sequentially acquired point-by-point, the sampling of the spatial dimensions is limited by keeping the total acquisition time

low, which leads to usually rather coarse maps.

In this paper we show that energy-filtered transmission electron microscopy (EFTEM) as an alternative acquisition technique enables us to directly image surface plasmons at low energies. As a parallel imaging technique, which gathers images using scattered electrons of a specific energy-loss range only, it achieves high spatial sampling easily and fast, while providing the same information content as STEM EELS [20, 21]. The energy resolution of the EFTEM technique is typically in the range of a few eV, but can be pushed to the sub-eV range if a small energy-filtering slit width and appropriate data correction schemes are used [22]. This enabled us to directly monitor surface plasmons at energies around or below 1 eV *without employing any deconvolution procedure*. We achieved image sizes of 512×512 pixels for exposure times on the minute scale.

Experiment.—In our experiments we used a Wien-filter monochromated FEI Tecnai F20 microscope with a High Resolution Gatan Imaging Filter and an UltraScan CCD camera [23]. The investigated specimen was a rod-shaped gold nanoparticle synthesized by a modification of the conventional citrate reduction of gold salt in water [24]. A holey carbon film was used as the sample support grid. Figure 1(a) displays the particle in a TEM bright field image. With the monochromated beam, the condenser lens was adjusted such that a homogeneous illumination of the particle could be achieved. An EFTEM image series was acquired via our customized acquisition script, which adapts exposure times and multiple frame read outs for each energy step to the encountered intensity situation [25]. We used an energy selecting slit width of 0.3 eV, and recorded the images in the energy range from 1.0 to 4.5 eV in 0.1 eV steps. The spatial sampling of the images was 512×512 pixels for a field-of-view of 456×456 nm, and the total acquisition time was 17 minutes. The raw data were then processed to correct for spatial drift, energy drift, and non-isochromaticity [22].

We first extracted, from single pixels of the EFTEM image series, energy-loss spectra at the three positions indicated in Fig. 1(a). Fig. 2(a) shows the corresponding spectra. For comparison, we also measured three EELS point spectra at approximately the same positions, which are shown in panel (b). All data are shown without background subtraction. In the spectra we observe three distinct peaks in the energy range below 3 eV, which we tentatively ascribe to the surface plasmon eigenmodes of the gold nanorod. This interpretation is supported by the EFTEM images of Fig. 1(b–d), taken at the energies of the peak maxima. The mode at 0.97 eV has its intensity maxima at the top and bottom end

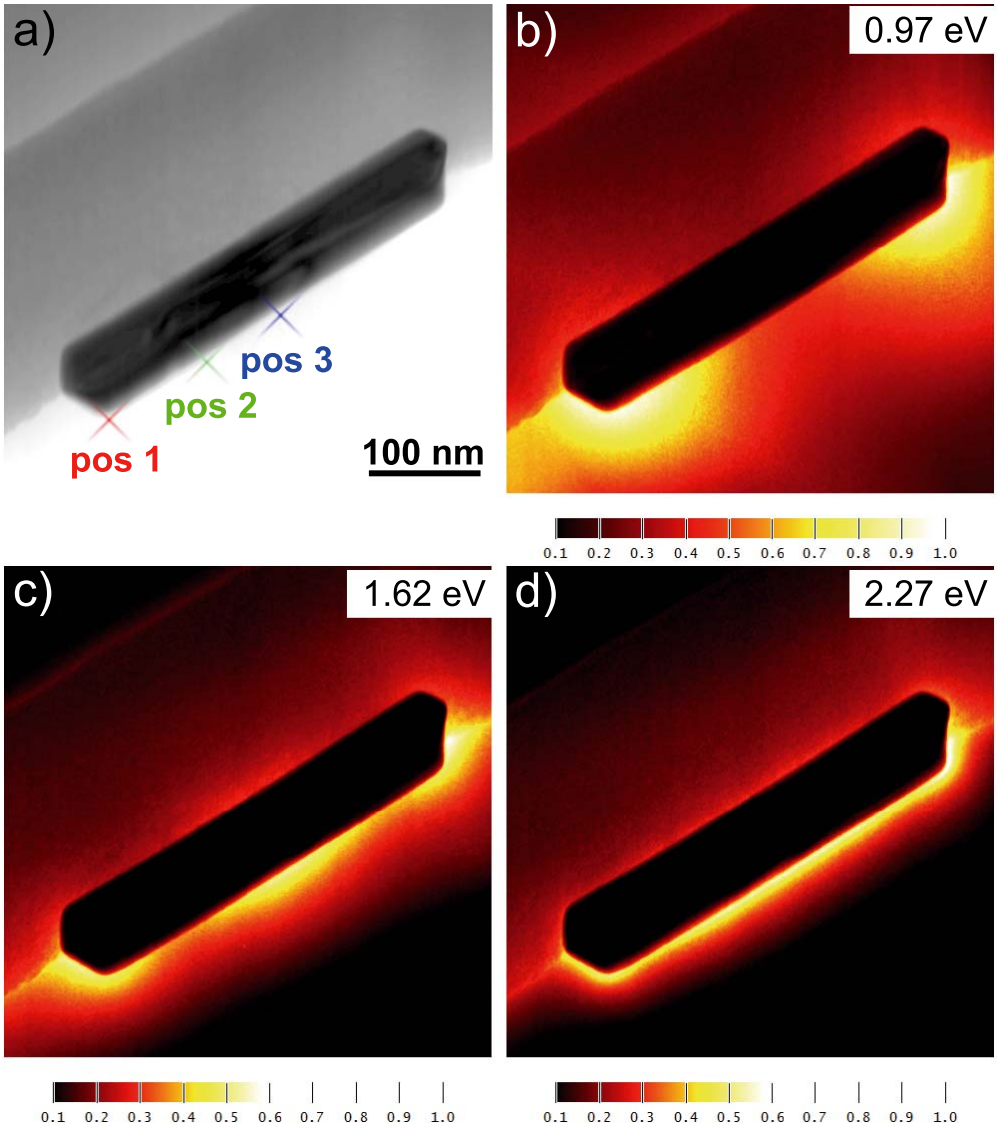

FIG. 1: (Color online) (a) TEM bright field image of rod-shaped gold nanoparticle, with approximately 400 nm length and 75 nm diameter. The markers indicate pixel positions at which EELS spectra in Fig. 2 have been extracted. (b–d) EFTEM images at given energy-loss values. Image intensities have been normalized with respect to the maximum intensity of panel (b). We use pseudocolor for better visibility. The EFTEM maps show the electromagnetic eigenmodes of the gold nanorod.

of the rod, reminiscent of a dipolar excitation, while the map depicted in panel (c) shows an additional peak in the central region of the nanorod, similar to the first excited mode of a linear antenna. Finally, the mode at 2.27 eV, panel (d), vaguely shows two maxima at approximately one and two thirds of the long nanorod axis. In all cases we observe a

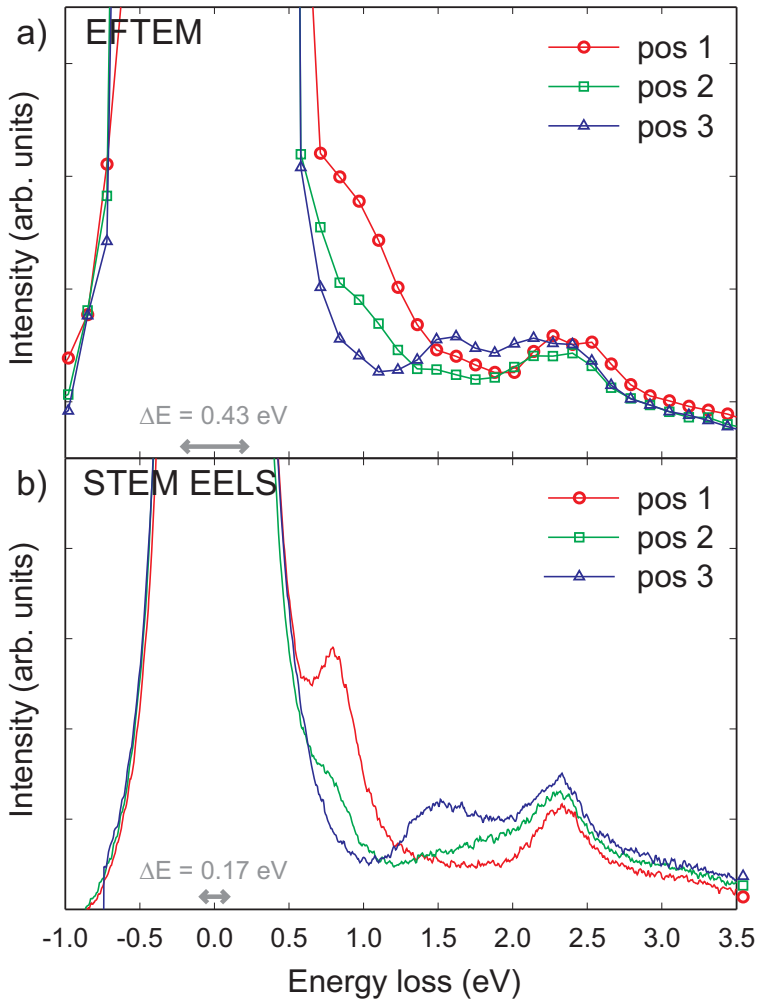

FIG. 2: (Color online) (a) Single-pixel extracted EELS spectra from EFTEM data at positions indicated in Fig. 1(a). (b) STEM EELS spectra acquired at the same sample positions. The arrows in the lower parts of the panels indicate the energy resolution of the data.

strongly reduced intensity at the sides of the carbon support, in comparison to the vacuum side, which we attribute to absorption losses of the electron beam in the carbon.

Theory.—To unambiguously interpret our experimental results, we additionally performed simulations using the boundary element method (BEM) approach [26, 27]. In our simulations we assume that a beam of 200 keV electrons passes in the vicinity of the metallic nanoparticle, as depicted in Fig. 3(a). For simplicity no penetrating trajectories were considered [13]. We model the gold nanoparticle as a rod with 400 nm length and 75 nm diameter, in accordance to the particle shape depicted in Fig. 1(a). The dielectric function of gold was extracted from optical data [28] and the refractive index of the surrounding

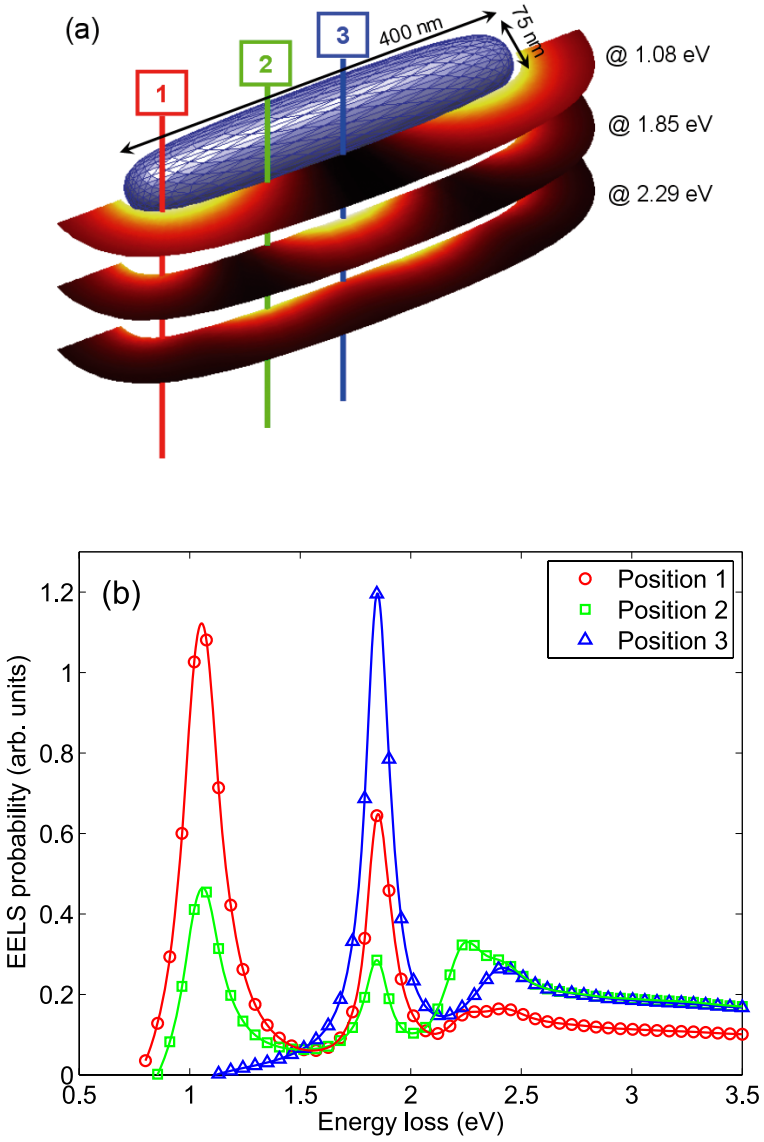

FIG. 3: (Color online) Results of BEM simulation. (a) Triangulated surface of rod-shaped nanoparticle and EFTEM maps as computed according to the prescription of Ref. [26]. The maps at the energies of 1.08 eV, 1.85 eV, and 2.29 eV have been displayed in pseudocolor scaled to match the data range of the 1.08 eV map. The loss rates for the 2.29 eV map have been multiplied by a factor of 5 for better visibility. The lines indicate the direction of the electron beam. (b) Energy-loss probability at the positions indicated in panel (a).

medium was set to one. The external excitation due to the electron beam is described by the Lièнard-Wiechert potentials [29]. We compute the dielectric response of the nanoparticle within the BEM framework by means of auxiliary surface charges and currents [26], which allow us to compute for a given frequency ω the induced electric field $\boldsymbol{E}_{\mathrm{ind}}[\boldsymbol{r}_e(t), \omega]$ at the

positions $\boldsymbol{r}_e(t)$ of the electron beam, and to express the energy loss probabilities according to [26]

$$\Gamma(\omega) = \frac{1}{\pi\omega} \int \mathrm{Re}\left\{ e^{-i\omega t} \boldsymbol{v} \cdot \boldsymbol{E}_{\mathrm{ind}}[\boldsymbol{r}_e(t), \omega] \right\} \, dt \,. \tag{1}$$

In our computational approach, we discretize the surface of the nanoparticle by a set of triangles, as shown in Fig. 3(a), and match the electromagnetic potentials at the triangle centers [27, 30]. For spherical nanoparticles we compared the loss probability $\Gamma(\omega)$ with the analytic results of Mie theory [31], and found excellent agreement between the numerical and analytic results.

Results of our BEM simulation are shown in Fig. 3. Plasmon peak maxima are found at the energy positions of 1.08 eV, 1.85 eV, and approximately 2.29 eV. The spatial intensity distribution of the plasmonic modes fits the experimental findings very well, giving evidence that the detected peaks in the EELS spectrum can be interpreted as the resonance modes of the plasmon oscillations of the gold nanoparticle. We attribute the differences between the energetic positions of the peak maxima in theory and experiment to our neglect of the holey carbon film in the simulations, which is expected to red-shift the peak maxima and to introduce an anisotropy in the simulated EFTEM maps. As regarding the peak at 2.29 eV, we find that it is strongly broadened. This is attributed to interband scatterings in gold, that take place above a threshold of approximately 2 eV. We also found that the EFTEM map of the 2.29 eV peak is smeared out when we compute the loss probabilities not at a single energy, but integrate over an energy window of 0.4 eV to simulate the effect of the limited energy resolution in the experiments.

Discussion.—The energy resolutions of both EFTEM and EELS is governed by the width of the ZLP. Surface plasmons of silver nanoparticles have been mapped by EELS in an energy regime above 1.70 eV, using cold field emission guns together with a deconvolution procedure applied to the raw data [13]. Surface plasmons of gold particles, which lie closer to the ZLP, are more difficult to observe and may need the resolution improvements of a monochromated system [32]. A monochromated beam has a truly symmetric energy distribution and no pronounced ZLP tails towards the low-loss regime, giving profound advantages over cold field emission guns in this energy range [33]. An analysis of the full width at half maximum of the ZLP, extracted from the data in the vacuum area, reveals for our setup an EFTEM energy resolution of 0.43 eV, to be compared with the EELS resolution of 0.17 eV. This higher spectral resolution of EELS is also apparent from Fig. 2, although in both cases

the different plasmonic eigenmodes, whose spectral widths are usually of the same order of magnitude, can be easily discriminated.

The advantage of EFTEM lies in its high spatial resolution over large field-of-views. It is important to realize that any attempt to obtain mapped EELS images with comparable spatial sampling is not simply more cumbersome or time-consuming, but is probably doomed to failure for the following reason. A difficulty for extreme low-loss mapping is posed by the strong intensity difference between the ZLP and the adjacent low-loss region, which challenges the dynamic range of the detector. The situation is even worse for a monochromated source, as the ZLP maximum becomes stronger with decreasing peak width. While it is possible to choose a setup which truncates the most intense parts of the ZLP by shifting the spectrum just across the edge of the detector, this technique relies on the stability of the system with respect to energy offsets over the time of acquisition. Considering the pixel dwell time of about 0.6 sec, which includes both the exposure time of 0.1 sec and the data readout of the detector, a spatial map of 512×512 data points would have taken close to 36 hours, during which energy drift must not have exceeded 0.5 eV. Such long time stability can hardly be achieved in any modern system. In contrast to the scanning beam approach, within EFTEM the energy dimension is sampled sequentially and the dynamic range problem close to the ZLP can be overcome by especially adapted acquisition routines [25]. A second advantage of EFTEM is its ability to rapidly image large areas at lower magnification, without tediously adjusting the electron beam to coarse sampling conditions. For instance, imaging the spatial distribution of the 1 eV peak alone would have required only 1 minute, thus demonstrating the unique capability of mapping large field-of-views with spatial resolution on the nanometer scale. Furthermore, in a scanned beam approach spatial drift during acquisition can lead to map distortions, which can not be corrected or even unambiguously identified from the data alone, whereas spatial consistence of EFTEM images is immediately evident.

In conclusion, we have shown that EFTEM imaging can be used to directly and efficiently visualize the electromagnetic eigenmodes of surface plasmons in metallic nanoparticles. The technique surpasses the spatial resolution of optical measurements by more than one order of magnitude and still allows for large field-of-views to be investigated within several minutes. Therefore, detailed studies of assembled particles or structured devices become available, bridging the gap between highly resolved local measurements, such as STEM

EELS, and optical microscopy techniques, which average over larger areas and smear out inhomogeneities on a nanometer scale. The technique can also be applied for fast screening of many particles with slightly different resonance frequencies, or to localize "hot spots" of strongest resonance in a device, prior to detailed local analysis. It could also be advantageous for beam sensitive samples, in those cases where high dose rates rather than the dose itself harms the specimen. Here a focused beam may alter the structure locally during the measurement, whereas rapid parallel illumination of the sample allows for snap shots of an undamaged specimen. It should be emphasized that a beam monochromator is paramount for resolving plasmon energies around and below 1 eV, which constitutes an important energy range for Au nanoparticles. We believe that EFTEM will not supersede the scanning EELS approach as a high-spatial-resolution and high-energy-resolution technique in general, but will amend its capabilities with respect to the spatial domain.

We thank Harald Ditlbacher and Franz Aussenegg for most helpful discussions. This work has been supported in part by the Austrian Science Fund FWF under project P18136–N13, and by the Zukunftsfonds Steiermark.

[1] E. Orzbay, Science **311**, 189 (2006).

[2] H. Atwater, Scientific American **296(4)**, 56 (2007).

[3] B. Lamprecht, J. R. Krenn, G. Schider, H. Ditlbacher, M. Salerno, N. Felidj, A. Leitner, F. R. Aussenegg, and J. C. Weeber, Appl. Phys. Lett. **79**, 51 (2001).

[4] S. I. Bozhevolnyi, V. S. Volkov, E. Deveaux, J. Y. Laluet, and T. W. Ebbensen, Nature **440**, 509 (2006).

[5] J. B. Pendry, Phys. Rev. Lett. **85**, 3966 (2000).

[6] H. J. Lezec, J. A. Dionne, and H. A. Atwater, Science **316**, 5823 (2007).

[7] A. Haes and R. P. V. Duyne, J. Am. Chem. Soc. **124**, 10596 (2002).

[8] P. Fortina, L. J. Kricka, D. J. Graves, J. Park, T. Hyslop, F. Tam, N. Halas, S. Surrey, and S. A. Waldman, JACS **124**, 10596 (2007).

[9] S. Nie and S. R. Emory, Science **275**, 1102 (1997).

[10] P. Anger, P. Bharadwaj, and L. Novotny, Phys. Rev. Lett. **96**, 113002 (2006).

[11] A. V. Akimov, A. Mukherjee, C. L. Yu, D. E. Chang, A. S. Zibrov, P. R. Hemmer, H. Park,

and M. D. Lukin, Nature **450**, 402 (2007).

[12] L. Novotny and B. Hecht, *Principles of Nano-Optics* (Cambridge University Press, Cambridge, 2006).

[13] J. Nelayah, M. Kociak, O. Stephan, F. J. Garcia de Abajo, M. Tence, L. Henrard, D. Taverna, I. Pastoriza-Santos, L. M. Liz-Marin, and C. Colliex, Nature Phys. **3**, 348 (2007).

[14] F. Ouyang, P. E. Batson, and M. Isaacson, Phys. Rev. B **46**, 15421 (1992).

[15] M. Bosman, V. J. Keast, M. Watanabe, A. I. Maaroof, and M. B. Cortie, Nanotechnology **18**, 165505 (2007).

[16] F. J. Garcia-de Abajo and M. Kociak, Phys. Rev. Lett. **100**, 106804 (2008).

[17] M. N'Gom, J. Ringnalda, J.F. Mansfield, A. Agarwal, N. Kotova, N.J. Zaluzec, and T.B. Norris, Nanoletters p. doi:10.1021/nl801504v (2008).

[18] D.A. Muller, and J. Silcox, Ultramicroscopy **59**, 195 (1995).

[19] R. Egerton, Journal of Electron Microscopy **48**, 711 (1999).

[20] A. Eggeman, P. J. Dobson, and A. K. Petford-Long, Journal of Applied Physics **101**, 024307 (2007).

[21] W. Grogger, M. Varela, R. Ristau, B. Schaffer, F. Hofer, and K. M. Krishnan, Journal of Electron Spectroscopy and Related Phenomena **143**, 139 (2005).

[22] B. Schaffer, G. Kothleitner, and W. Grogger, Ultramicroscopy **106**, 1129 (2006).

[23] G. Kothleitner and F. Hofer, Micron **34**, 211 (2003).

[24] J. Turkevich, P. C. Stevenson, and J. Hillier, Discussion of the Faraday Society **11**, 9 (1951).

[25] G. Kothleitner and B. Schaffer, Microscopy and Microanalysis **13**, 156 (2007).

[26] F. J. Garcia de Abajo and A. Howie, Phys. Rev. B **65**, 115418 (2002).

[27] U. Hohenester and J. R. Krenn, Phys. Rev. B **72**, 195429 (2005).

[28] P. B. Johnson and R. W. Christy, Phys. Rev. B **6**, 4370 (1972).

[29] J. D. Jackson, *Classical Electrodynamics* (Wiley, New York, 1999).

[30] U. Hohenester and A. Trügler, to appear in IEEE J. Sel. Top. Quantum Electon. (2008); arXiv:0801.3900.

[31] F. J. Garcia de Abajo, Phys. Rev. B **59**, 3095 (1999).

[32] B. Schaffer, K. Riegler, G. Kothleitner, W. Grogger, and F. Hofer, Micron p. doi:10.1016/j.micron.2008.07.004 (2008).

[33] K. Kimoto, G. Kothleitner, W. Grogger, Y. Matsui, and F. Hofer, Micron **36**, 185 (2005).